

# Selective Structured State Space for Multispectral-fused Small Target Detection

Qianqian Zhang<sup>1,2\*</sup> Weijun Wang<sup>3</sup> Zihan Wang<sup>5</sup> Li Zhou<sup>1</sup> Hao Zhao<sup>3</sup>  
Junshe An<sup>1,4</sup> Yunxing Liu<sup>3</sup>

<sup>1</sup>National Space Science Center, Chinese Academy of Sciences, China

<sup>2</sup>School of Computer Science and Technology, University of Chinese Academy of Sciences, China

<sup>3</sup>Institute for AI Industry Research (AIR), Tsinghua University, China

<sup>4</sup>School of Astronomy and Space Science, University of Chinese Academy of Sciences, China

<sup>5</sup>School of Computing, National University of Singapore

zhangqianqian21@mails.ucas.ac.cn wangweijun@air.tsinghua.edu.cn zhouli@nssc.ac.cn

liuyunxin@air.tsinghua.edu.cn zhaohao@air.tsinghua.edu.cn anjunshe@nssc.ac.cn

zihan.wang@u.nus.edu

## Abstract

*Target detection in high-resolution remote sensing imagery faces challenges due to the low recognition accuracy of small targets and high computational costs. The computational complexity of the Transformer architecture increases quadratically with image resolution, while Convolutional Neural Networks (CNN) architectures are forced to stack deeper convolutional layers to expand their receptive fields, leading to an explosive growth in computational demands. To address these computational constraints, we leverage Mamba’s linear complexity for efficiency. However, Mamba’s performance declines for small targets, primarily because small targets occupy a limited area in the image and have limited semantic information. Accurate identification of these small targets necessitates not only Mamba’s global attention capabilities but also the precise capture of fine local details. To this end, we enhance Mamba by developing the Enhanced Small Target Detection (ESTD) module and the Convolutional Attention Residual Gate (CARG) module. The ESTD module bolsters local attention to capture fine-grained details, while the CARG module, built upon Mamba, emphasizes spatial and channel-wise information, collectively improving the model’s ability to capture distinctive representations of small targets. Additionally, to highlight the semantic representation of small targets, we design a Mask Enhanced Pixel-level Fusion (MEPF) module for multispectral fusion, which enhances target features by effectively fusing visible and infrared multimodal information.*

## 1. Introduction

Target detection is an important field that has been widely utilized in urban vehicle detection [41], wildlife observation [30] and agricultural pest detection [42], etc. These application scenarios often face challenges related to the low detection performance of small targets, even with the high resolution of the entire image. Furthermore, with advancements in remote sensing technology, image resolution continues to improve. However, existing CNN and Transformer networks exhibit low real-time computing efficiency when processing high-resolution images. Introducing a selective structured state space model (Mamba) with linear time complexity to target detection tasks is a promising choice to decrease the computational cost for high-resolution images.

However, simply applying Mamba (e.g., Vmamba [29] and MambaYOLO [43]) for small target detection shows unsatisfactory accuracy. This is primarily due to two key challenges. First, small targets occupy only a minimal percentage of the entire image, with limited semantic information available for detection. Second, the vast amount of background noise may *drown out* the subtle yet crucial clues of small targets, which makes existing feature extraction networks hard to effectively capture the distinctive characteristics of small targets. Therefore, enhancing small target saliency in complex backgrounds is crucial for improving detection accuracy, which requires better networks and strategies for feature extraction and noise suppression.

Multispectral fusion detection, such as visible-infrared fusion, enhances small-target detection by leveraging complementary spectral information. Visible spectra provide texture and color details, while infrared captures thermal radiation, invariant to lighting. This synergy highlights crucial high-frequency features like edges and fine details, im-

\*This work was completed during Qianqian Zhang’s research internship at the Institute for AI Industry Research (AIR), Tsinghua University.

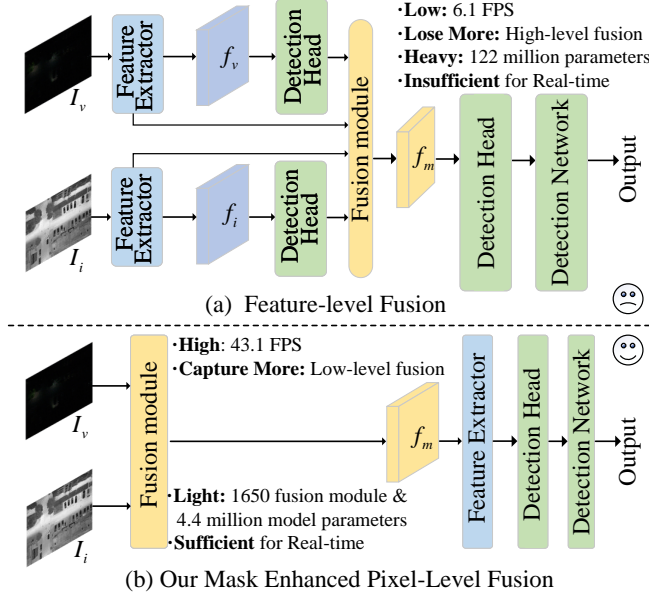


Figure 1. The comparison of previous multispectral fusion detection methods (a) and Ours (b).

proving detection accuracy. Fusion methods include pixel-level [9, 51, 55] and feature-level fusion [33, 45].

However, existing methods face deployment challenges due to high computational costs. *e.g.*, The Mask-guided Mamba Fusion model (MGMF) [41] has 122 million parameters and runs at just 6.1 FPS, limiting its suitability for mobile or real-time applications, as shown in Fig. 1 (a). Lightweight pixel-level fusion is a promising solution, but current approaches suffer from spatial misalignment caused by registration errors, leading to blurred or misplaced details. Moreover, aligning multi-modal features at the pixel level is difficult, exacerbating feature loss. To address these issues, we propose a mask generation module to learn aligned spatial semantics and a feature fusion module to reduce redundancy and enhance pixel-level fusion quality, as shown in Fig. 1 (b).

To address the challenges in small target detection, this work proposes a model based on a selective structured state space model (Mamba) and multispectral fusion. We tackle three key problems: 1) limited feature extraction and localization for small targets due to their minimal area, semantic information, and interference from complex background occlusion; 2) inefficient fusion of visible and infrared spectral information at the pixel level; and 3) high computational costs of traditional methods when processing high-resolution images. We leverage Mamba’s global attention and design the Enhanced Small Target Detection (ESTD) module to enhance feature extraction, while introducing the Convolutional Attention Residual Gate (CARG) Block, built upon Mamba, to emphasize spatial and channel-wise

information, reducing background noise and improving robustness. We also propose the lightweight Mask Enhanced Pixel-level Fusion (MEPF) module for efficient multispectral fusion. Additionally, we use Mamba’s linear complexity to efficiently process high-resolution images. Experimental results demonstrate that we achieve high-precision performance with minimal computational cost.

Our contributions are summarized as follows:

- We propose the MEPF module for efficient multispectral fusion, which improves fusion quality with only 1650 parameters (0.0063MB), enabling lightweight deployment on edge devices.
- The ESTD and CARG modules are proposed to improve the Mamba network, enhancing the model’s capability to effectively capture visual clues of small targets.
- Our method achieves high-precision on DroneVehicle and VEDAI datasets, balancing detection accuracy and real-time inference speed. The experiments validate its effectiveness in multimodal fusion and small target detection.

## 2. Related Work

**High-resolution image target detection.** As image resolution continues to increase, computational efficiency for high-resolution detection has become a focal point. CNN [15, 17, 38] models are inefficient for high-resolution images due to their convolution operations, which increase computation drastically with resolution. Deeper networks are often needed for global information. Vision Transformer [6] has approached top performance in image recognition but is limited by quadratic complexity.  $C^2Former - S^2ANET$  [49] (based on Transformer) can’t handle resolutions above  $1092 \times 1092$  pixels, while DMM [56] (based on Mamba) can handle  $3016 \times 3016$  pixels. Vision Mamba [57] and VMamba [29] use Mamba’s linear complexity, showing advantages in high-resolution processing. Vision Mamba is  $2.8 \times$  faster and saves 86.8% GPU memory than DeiT [19] on  $1248 \times 1248$  images. Mambaout [48] also highlights Mamba’s potential for long sequence tasks. Traditional methods (CNN, Transformer) overlook the challenges of target detection in high-resolution images, while our approach embeds Mamba into the feature extraction backbone for efficient high-resolution image detection.

**Small target detection.** In this work, we adopt the definition of small targets from Gao *et al.* [8], where the ratio of the bounding box’s width and height to those of the image is less than 0.1. Mamba-based target detection models exhibit low accuracy in detecting small targets. This issue is particularly prevalent in remote sensing, which has sparked research interest [3, 40, 54, 56]. This is because the model will focus on all areas of the entire image under global attention, but small target detection usually requires finer local details. The YOLO series is the most popular real-time target detection algorithm and widely regarded as the cur-

rent standard in the field. Small target detection based on YOLO has been extensively studied [40, 44, 47, 53]. However, these methods still exhibit low detection performance when relying on the YOLO model based on a CNN architecture to detect small targets directly. This is because local attention, when processing small targets, loses information due to changes in the location of the small target within the local area. Existing methods often neglect balancing global and local attention in small target detection. Our approach enhances Mamba’s global attention with local modules, capturing both contextual dependencies and fine-grained details. This dual mechanism ensures comprehensive feature representation, overcoming the limitations of relying solely on global attention.

**Multispectral fusion target detection.** Multispectral fusion methods can be roughly categorized into pixel-level, feature-level, and decision-level fusion. Feature-level fusion is the fusion of extracted image features. MGMF [41] uses candidate regions of one modality to guide feature extraction of another modality for cross-modal feature fusion, but its performance falls short of real-time processing. Decision-level image fusion is done before getting the final detection result; this method has lower performance. Pixel-level fusion is performed on the pixels of the source image to obtain the fused image. Its advantage is that it preserves the spectral and spatial characteristics of the input image, generating a fused image that contains more information than the input images. SuperYOLO [51] improves target detection through pixel-level multimodal fusion. Although the method has a small number of parameters, it is expected to be improved in terms of multispectral feature fusion for small targets. Existing methods overlook the trade-off between fusion quality and computational efficiency for small targets; our approach resolves this through a lightweight fusion module that enhances feature representation while preserving real-time capability.

### 3. Preliminaries

This section reviews State Space Models (SSM) *i.e.*, Mamba [11] as a foundation for understanding linear complexity problems. Subsequently, we present the principles of the VMamba [29] image detection process.

#### 3.1. Mamba

SSM maps an input sequence  $x(t) \in \mathbb{R}$  to an output sequence  $y(t) \in \mathbb{R}$  through a hidden state  $h(t) \in \mathbb{R}^N$ . In the 1-D situation, discrete SSM transform sequences as linear ordinary differential equations (ODEs):

$$\begin{aligned} h'(t) &= \mathbf{A}h(t) + \mathbf{B}x(t), \\ y(t) &= \mathbf{C}h(t). \end{aligned} \quad (1)$$

where  $\mathbf{A} \in \mathbb{R}^{N \times N}$  is the state transition matrix, while  $\mathbf{B} \in \mathbb{R}^{N \times 1}$  is the input coefficient vector, and  $\mathbf{C} \in \mathbb{R}^{1 \times N}$  serves

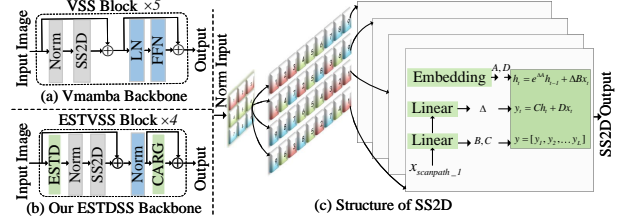


Figure 2. The comparison of Vmamba (a) and Our method (b). And structure of SS2D (c). Four different scan paths are set for traversing, and each sequence is processed independently.

as the output coefficient vector.

Mamba [5, 10] is an SSM-based model with selective state space. To improve expressiveness and flexibility, Mamba proposes to make  $\mathbf{A}$  and  $\mathbf{B}$  dynamically dependent on inputs, enabling an input-aware selective mechanism for better state space modeling. Mamba approximates this ODE by discretizing  $\mathbf{A}$  and  $\mathbf{B}$  with a time step parameter  $\Delta$  using a zero-order hold trick:

$$\begin{aligned} \bar{\mathbf{A}} &= \exp(\Delta \mathbf{A}), \\ \bar{\mathbf{B}} &= (\Delta \mathbf{A})^{-1}(\exp(\Delta \mathbf{A}) - \mathbf{I}) \cdot \Delta \mathbf{B}. \end{aligned} \quad (2)$$

After discretization, Eq. (3) is reformulated:

$$\begin{aligned} h_k &= \bar{\mathbf{A}}h_{k-1} + \bar{\mathbf{B}}x_k, \\ y_k &= \mathbf{C}h_k. \end{aligned} \quad (3)$$

It is an efficient recursive model due to its finite state design, enabling constant-time reasoning and linear-time training. It is worth noting that Mamba’s sequential scanning, designed for ordered text data, is inherently unsuitable for images due to their lack of inherent order.

#### 3.2. VMamba

Vmamba takes into account that visual data itself is unordered and contains spatial information about local textures and global structures. The 2D Selective Scan (SS2D) module in its core Visual State Space (VSS) Block module solves the sequential scanning problem, as shown in Fig. 2 (c). VSS Block improves computational efficiency by using network branches and two residual module structures instead of multiplicative branches, as shown in Fig. 2 (a). Our method further enhances the core structure of Mamba to address the unique characteristics of small targets, as shown in Fig. 2 (b).

### 4. Method

This section outlines the architecture and specific design elements of our approach. We present a multimodal fusion real-time small target recognition network tailored for remote sensing scenarios:  $S_6^4$ -MSTD, as shown in Fig. 3.

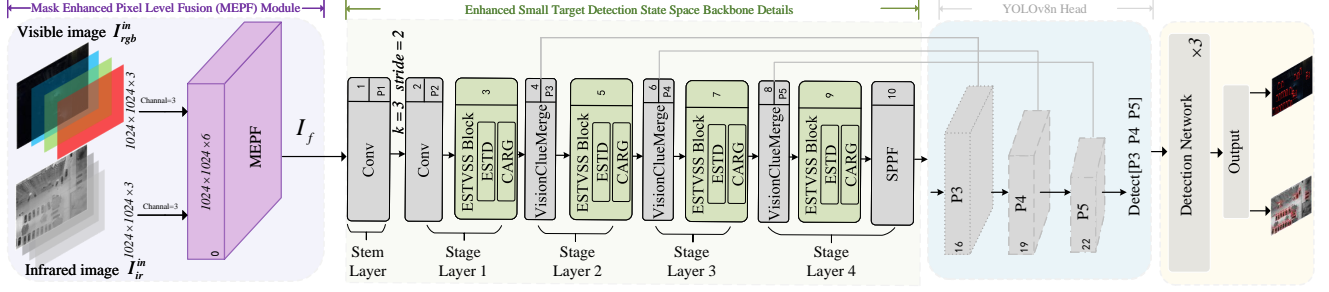


Figure 3. An overview of  $S_6^4$ -MSTD. It consists of four components which are the Mask Enhanced Pixel-level Fusion Module, the Enhanced Small Target Detection State Space Backbone, the YOLOv8n Head, and the Detection Network. The captured visible and infrared images are firstly fused by the MEPF module to generate the fused images  $I_f$ . The task of the backbone module is to extract features from the fused images. We introduce the ESTD module and CARG module to enhance Mamba’s feature extraction capability specifically for small targets. After this, the head network fuses the features extracted at different stages. Finally, it is fed into the detection network to get the detection results.

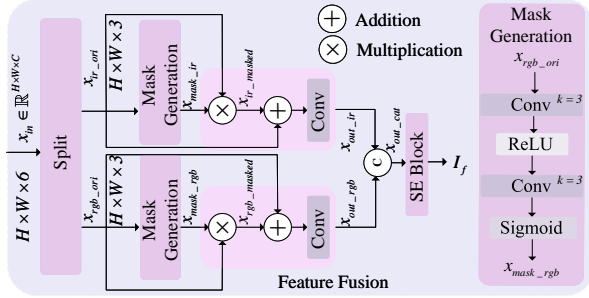


Figure 4. The architecture of the mask enhanced pixel-level fusion module consists of a split module, a mask generation module, and a feature fusion module, where  $x_{in}$  is the input,  $I_f$  is the pixel-level fused image, and  $k = 3$  indicates a convolutional kernel size of  $3 \times 3$ . We will detail the implementation in 4.1.

$I_{rgb}^{in} \in \mathbb{R}^{H \times W \times 3}$  is the visible modal picture, and the infrared modal picture is  $I_{ir}^{in} \in \mathbb{R}^{H \times W \times 3}$ . These images are taken as input to  $S_6^4$ -MSTD.

#### 4.1. Mask Enhanced Pixel-level Fusion

To generate a high-quality fusion image  $I_f$ , we design the MEPF module. Fig. 4 shows our MEPF module implementation in detail. The input is  $x_{in} \in \mathbb{R}^{H \times W \times 6}$ . Visible modal feature  $x_{rgb\_ori} \in \mathbb{R}^{H \times W \times 3}$  and infrared modal feature  $x_{ir\_ori} \in \mathbb{R}^{H \times W \times 3}$  are obtained after split module.

When the data of different modes are fused, they need to be transformed into a unified feature space or representation, which misses some spatial structure information or depth information. To address this problem, we design the mask generation module shown in Eq. (4) to generate the initial mask  $x_{mask\_rgb}$  and  $x_{mask\_ir}$ .

$$x_{mask\_rgb} = \sigma_{Sig}(C_3(ReLU(C_3(x_{rgb\_ori})))) \quad (4)$$

where  $ReLU$  is ReLU activation [1],  $\sigma_{Sig}$  is Sigmoid functions [7] and  $C_3$  is  $Conv_{3 \times 3}$  [39].

Each modality’s data itself has some redundant information, *e.g.*, background information and repetitive textures. If the redundant information is not screened and removed effectively in multi-modal fusion, the computational complexity of the fused feature would increase. To address this, we design a feature fusion module (shown in Eq. (5)) that selectively filters redundant information while preserving critical features.

$$x_{out\_rgb} = C_3(x_{rgb\_ori} + x_{rgb\_ori} \otimes x_{mask\_rgb}) \quad (5)$$

where  $\otimes$  is the element-wise multiplication.

Furthermore, we propose a spatial feature compression method (depicted in Eq. (6)), which compresses multi-modal 2D feature channels into a compact modal factor  $M \in \mathbb{R}^{(C_1+C_2) \times 1 \times 1}$ , effectively reducing redundancy while maintaining essential information.

$$M = \sigma_{Sig}(FC(ReLU(FC(M')))), \\ M' = Avg(Cat[x_{out\_rgb}, x_{out\_ir}]) \quad (6)$$

where  $FC$  is the fully connected layer [23],  $Avg$  is the global average pooling [27]. The factor  $M$  captures a global receptive field, with its output dimension matching the input feature channels. This enables layers near the input to gain broader context awareness, enhancing their understanding of contextual information. The result is shown in Eq. (7).

$$I_f = M \cdot (Cat[x_{out\_rgb}, x_{out\_ir}]) \quad (7)$$

Fig. 9 compares the feature map visualizations of our MEPF module and baseline. The baseline [51] uses a  $1 \times 1$  convolution to generate a mask. The simple  $1 \times 1$  convolution is unable to capture the complex spatial relationships. In contrast, our MEPF uses two  $3 \times 3$  convolution layers and a ReLU activation function to generate masks, capable of learning small target-matched spatial features. In the mask application mode, the baseline multiplies the mask with the

features after 0.5 times scaling. This scaling results in information loss. In contrast, we apply the mask directly to the original feature map and use the Sigmoid function to rescale the mask value to  $[0, 1]$ . We avoid additional scaling operations, thereby making better use of the original features.

## 4.2. Enhanced Small Target Visual State Space

The design of the backbone is based on two main considerations. On one hand, the backbone should achieve high performance in processing high-resolution images. On the other hand, it should be able to better capture the feature information of small targets.

To address the problem that the computational complexity of the Transformer architecture grows quadratically with the increase of image resolution, whereas CNN requires deeper structures to handle high-resolution images, we choose to introduce the selective structured state space model (Mamba) with linear time complexity into the visual backbone to solve the computational constraints of high-resolution image detection.

However, Mamba’s performance declines for small targets due to its reliance on long-range dependencies, which may weaken local feature representation. In high-resolution images, small targets occupy a minimal proportion, resulting in weak features that are easily overwhelmed by complex background information. To address this, we design the Enhanced Small Target Visual State Space (ESTVSS) Block (as shown in Fig. 5), a tailored modification to the Mamba architecture for small target detection. The ESTD block enhances local attention, capturing fine-grained details that global attention often misses. The CARG block further strengthens spatial and channel attention, effectively distinguishing small targets from complex backgrounds. Together, these modifications enable the ESTVSS Block to overcome the limitations of Mamba in small target scenarios.

The input tensor  $X$  is processed by the Input Projection module to obtain  $X_{proj}$  Eq. (8).

$$X_{proj} = SiLU(BN(C_1(X))) \quad (8)$$

where  $C_1$  is  $Conv_{1 \times 1}$  [39].  $SiLU$  is SiLU activation [7]. BN is Batch normalization layer [20].

**Enhanced Small Target Detection Module.** The receptive field size crucially influences small target detection accuracy. Relying solely on global attention risks missing critical small target features due to insufficient focus, while using only local attention in complex backgrounds leads to interference from similar textures. Global attention aids in target localization through contextual understanding, whereas local attention excels at extracting detailed features. Combining global attention, which captures overall image context, with local attention, focused on fine-grained details, is beneficial for precision. Therefore, we introduce

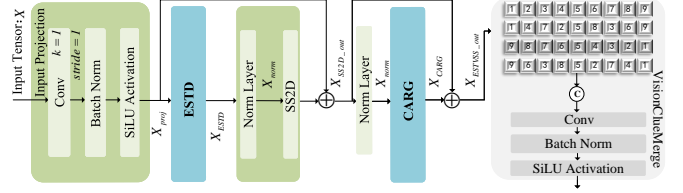


Figure 5. Structure of ESTVSS Block and VisionClueMerge. MEFP module generates  $I_f$ . After that, we use ESTVSS Block for feature extraction. VisionClueMerge is used to merge and stitch tensors. The ESTD module and the CARG module are used to enhance the detection of small targets.

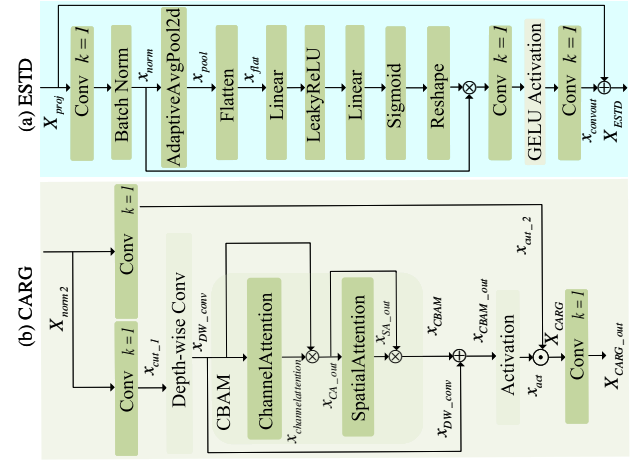


Figure 6. Structure of ESTD block and CARG block.

the ESTD Block, a tailored modification to the Mamba architecture, specifically designed to optimize the receptive field for small target detection by enhancing local attention. As shown in Fig. 6 (a) and Eq. (9), this modification addresses the unique challenges of small targets, ensuring precise feature extraction in complex scenarios.

$$X_{ESTD} = C_1(GELU(C_1(SE(BN(C_1(X_{proj})))))) \quad (9)$$

where  $GELU$  is GELU activation [24]. SE is Squeeze-and-Excitation block [16].

**Convolutional Attention Residual Gate Module.** The existing approach faces two primary limitations: 1) difficulty in capturing subtle yet critical small target features, such as shape, color, and texture; and 2) inability to handle complex background occlusion, which significantly reduces detection accuracy. To address these challenges, we introduce the CARG module, a tailored enhancement to the Mamba architecture designed specifically for small target detection. The CARG module augments the model’s channel and spatial attention capabilities, as illustrated in Fig. 6 (b), enabling robust feature extraction in complex scenarios. The CARG module’s channel attention mechanism identifies and emphasizes channels containing critical seman-

tic information, such as shape and color, while suppressing irrelevant background channels. This selective weighting helps the model focus more on key small target features, reducing the impact of complex backgrounds. Complementing this, the spatial attention component enhances the model’s ability to distinguish small targets from occluding backgrounds. Together, these mechanisms enable the CARG module to effectively address the unique challenges of small target detection in high-resolution imagery, making it a pivotal enhancement to the Mamba architecture.

$$x_{channelattention} = \sigma_{Sig}(x_{out_{avgpool}} \otimes x_{out_{maxpool}}) \quad (10)$$

$$x_{out_{avgpool}} = C_1(ReLU(C_1(f_{AP}(x_{DW_{conv}}))) \quad (11)$$

$$x_{out_{maxpool}} = C_1(ReLU(C_1(f_{MP}(x_{DW_{conv}}))) \quad (12)$$

where  $f_{MP}$  is 2D adaptive max pooling [35].  $f_{AP}$  is 2D adaptive average pooling [46].  $x_{DW_{conv}}$  is the feature processed by Depth-wise separable convolution [4].

The primary function of Spatial Attention is to enhance small target localization by suppressing background interference. The area occupied by small targets in the image is usually small and they are easily obscured by the surrounding background. The Spatial Attention mechanism can identify the specific spatial region where a small target is located through the analysis of spatial locations, and assign a higher weight to this region so that the model can focus more attention on the spatial location of the small target in subsequent processing. Meanwhile, the weight of the surrounding background region is reduced, thereby shifting the model’s attention from the background region to the small - target region, reducing the interference of the background on small target detection, and enabling the model to process the relevant information of small targets more accurately.

$$x_{mean} = ChannelMean(x_{CA_{out}}) \quad (13)$$

$$x_{max} = ChannelMax(x_{CA_{out}}) \quad (14)$$

$$x_{spatialattention} = \sigma_{Sig}(C_1(Cat[x_{mean}, x_{max}])) \quad (15)$$

where  $x_{CA_{out}}$  is shown in Fig. 6 (b).

## 5. Experiments

We first present the implementation details of  $S^4$ -MSTD. Then, we evaluate its performance on the challenging DroneVehicle [36] and VEDAI [32] datasets. Finally, we discuss the limitations of our approach.

### 5.1. Datasets

**DroneVehicle dataset** [36] is currently the largest benchmark dataset in the field of cross-modal vehicle small target detection. The dataset consists of 56,878 images, *i.e.*, 28,439 pairs of visible infrared images. Five types of vehicles are involved, including cars, buses, trucks, vans, and

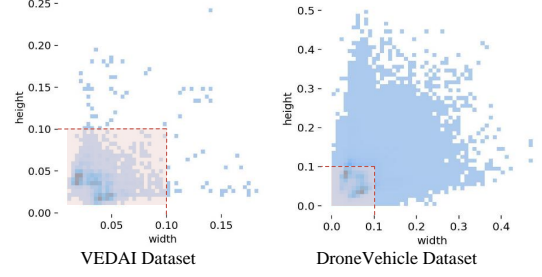


Figure 7. Distribution of target sizes in the datasets. The majority of targets in the VEDAI dataset [32] meet the definition of small targets (with a size ratio below 0.1) [8], while only a small portion of targets in the DroneVehicle dataset [36] satisfy this criterion.

lorries. Among them, the training set, validation set, and test set consist of 17,990, 1,469, and 8,980 images. The image size is  $840 \times 712$  pixels. Each image is captured by a camera-equipped drone in different scenes and under different lighting conditions, with a large number of nighttime scenes included, thus ensuring the diversity and complexity of the DroneVehicle dataset.

**VEDAI dataset** [32] is designed for vehicle detection in high-resolution aerial imagery, including complex background environments, *e.g.*, grasslands, highways, mountains, and urban landscapes. The dataset consists of 1246 pairs of RGB and infrared images with resolutions of  $1024 \times 1024$  and  $512 \times 512$  pixels. According to [32], small object detection achieves only 10% to 20% recall at 0.01 FPPI, with most false positives from background areas. This highlights the challenge of detecting small objects in complex scenes. In our experiments, we use the  $1024 \times 1024$  version to evaluate our method’s robustness.

### 5.2. Training details

The experiments are carried out on a single NVIDIA RTX A100 GPU with 80 GB memory. We implement our algorithm with PyTorch and SGD optimizer [37] with a momentum of 0.937 and a weight decay of 0.0005. The learning rate is set to 0.01. The batch size is 8. The training epochs are set to 300. We use the ground truth of the IR images as the training label, owing to the more comprehensive target annotations available in the IR modality. In addition, to ensure that the model is lightweight, we refer to the model parameter settings of YOLOv8n [22], *i.e.*, the model’s depth is set to 0.33 and the model’s width is set to 0.25.

### 5.3. Assessment Indicators

Mean Average Precision (mAP) is utilized as a precision metric to assess the performance of the various methods. Additionally, Frames Per Second (FPS) and parameter sizes serve as quantifiable measures to evaluate the real-time capability and computational expenditure of the model.

## 5.4. Results Comparisons

To evaluate the detection accuracy of small targets, we use the VEDAI dataset [32], which contains mostly small targets (size ratio below 0.1) [8]. Additionally, to validate the applicability of our method in scenarios with mixed small and large targets, we evaluate the DroneVehicle dataset [36]. The experimental results on the VEDAI dataset [32] show that our method achieves 81.2% mAP, a state-of-the-art performance in this challenging benchmark test, as shown in Tab. 1.

Method	Car	Pickup	Camping	Truck	Other	Tractor	Boat	Van	mAP <sub>50</sub> (%)↑
ZAQ[CVPR'21] [28]	88.0	85.8	70.5	<u>79.4</u>	45.1	<u>88.1</u>	67.7	<u>84.0</u>	76.1
AFD[AAAI'21] [21]	88.5	85.5	71.3	73.5	58.7	<b>89.1</b>	59.7	80.4	75.8
ReviewKD[CVPR'21] [2]	85.1	84.5	72.8	73.6	58.4	84.3	68.6	<b>94.0</b>	77.7
YOLOFusion[PR'22] [31]	<u>91.7</u>	<u>85.9</u>	78.9	78.1	54.7	71.9	71.1	75.2	<u>78.6</u>
SuperYOLO[TGRS'23] [51]	91.1	85.7	<u>79.3</u>	70.2	57.3	80.4	60.2	76.5	75.9
OST[TGRS'23] [52]	91.1	<b>87.7</b>	74.9	<b>82.2</b>	<u>64.6</u>	84.9	60.2	82.9	<u>78.6</u>
DMM[arxiv'24] [56]	84.2	78.8	79.0	65.7	56.2	72.3	<u>72.3</u>	72.5	75.0
ICAFusion[PR'24] [34]	-	-	-	-	-	-	-	-	76.6
C <sup>2</sup> Former-S <sup>2</sup> ANet[TGRS'24] [49]	76.7	68.7	63.2	52.0	41.9	59.8	43.3	48.0	55.6
Ours	<b>91.8</b>	69.3	<b>82.3</b>	78.5	<b>84.6</b>	85.8	<b>75.6</b>	81.6	<b>81.2</b>

Table 1. Mean Average Precision (mAP) comparison of different methods on the VEDAI dataset. The best result is shown in **bold** and the second best is shown with under line.

As shown in Tab. 2, multispectral (IR+RGB) fusion on the DroneVehicle dataset improves detection accuracy compared to single-modality (IR or RGB). Our method, as highlighted in Tab. 3, excels in accurately identifying small targets, such as cars, within the mixed-size target DroneVehicle dataset. It outperforms MGMF [41] with a  $6.07 \times$  speedup and a  $27.29 \times$  reduction in model size. While it exhibits a marginally lower overall accuracy, it achieves superior performance specifically for small cars. This indicates it also demonstrates powerful adaptability in scenarios with mixed-size targets, while ensuring excellent real-time performance and a lightweight model.

As shown in Fig. 8, YOLOv8n with CNN as the main structure has detection errors on all 7 images (a)-(g). C<sup>2</sup>Former-S<sup>2</sup>ANet [49] with Transformer as the main structure has detection errors in (b) and (d)-(f) on the 4 images. Ours only has detection errors on 2 images. On analysis, (d) is due to the similarity in shape of the Freight Car and Car in this image and the relative concentration of multiple targets. (f) is a picture in a high-speed acquisition state where the image itself is blurred and obscured by trees.

## 5.5. Ablation Study

**Effect of MEPF module.** Our MEPF module can produce a higher quality fusion image. As shown in Tab. 4 (first and second lines), it improves the baseline model's performance by +2.9%. The baseline model consists of three components: the VMamba [29] backbone, traditional pixel-level fusion [51], and the YOLOv8n head [22], as illustrated in Fig. 9. Our MEPF module generates higher-quality fu-

Method	Modality	Car	Truck	Bus	Van	FreightCar	mAP <sub>50</sub> (%)↑
Oriented RepPoints [25]	IR	89.9	55.6	89.1	48.1	<u>57.6</u>	68.0
S <sup>2</sup> ANet [13]		89.9	54.5	88.9	48.4	55.8	67.5
LSKNet-OB [26]		<u>90.3</u>	<b>73.3</b>	89.2	<u>53.2</u>	<b>57.8</b>	<b>72.8</b>
ReDet [14]		90.0	61.5	<u>89.5</u>	46.6	55.6	68.6
Ours		<b>96.8</b>	<u>68.3</u>	<b>93.9</b>	<b>59.5</b>	44.0	<u>72.5</u>
Oriented RepPoints [25]	RGB	84.4	55.0	85.8	46.6	39.5	<u>62.3</u>
S <sup>2</sup> ANet [13]		80.0	54.2	84.9	43.8	<u>42.2</u>	61.0
LSKNet-OB [26]		<u>89.5</u>	<u>70.0</u>	<u>89.4</u>	56.9	<b>51.8</b>	<b>71.5</b>
ReDet [14]		69.5	47.9	31.0	<b>77.0</b>	29.0	51.0
Ours		<b>94.6</b>	<b>70.5</b>	<b>94.2</b>	<u>61.3</u>	36.9	<b>71.5</b>
DPDETR [12]	RGB+IR	90.3	<u>78.2</u>	90.1	64.9	<u>75.7</u>	<u>79.8</u>
DMM [56]		90.4	<b>79.8</b>	68.2	<b>89.9</b>	68.6	79.4
S <sup>2</sup> ANet [13]		90.0	64.5	88.2	53.2	61.7	71.5
TSFADet [50]		89.9	67.9	89.9	54.0	63.7	73.1
C <sup>2</sup> Former-S <sup>2</sup> ANet [49]		90.2	68.3	89.8	58.5	64.4	74.2
UA-CMDet [36]		87.5	60.7	87.1	37.9	46.8	64.0
MKD [18]		<u>93.5</u>	62.5	<u>91.9</u>	44.5	52.7	69.0
MGMF [41]		91.4	70.1	91.1	69.4	<b>78.5</b>	<b>80.2</b>
Ours		<b>96.8</b>	69.2	<b>93.1</b>	60.4	52.8	74.5

Table 2. mAP comparison of different methods on the DroneVehicle dataset. The target pixel sizes are sorted as: **Car** < Bus < Van < Freight Car < Truck. For the smallest targets like cars, ours has better performance than the CNN architecture (UA-CMDet [36], MKD [18]), Transformer architecture (DPDETR [12]), and other models based on Mamba architecture (DMM [56], MGMF [41]).

Method	Size (MB)↓	Speed (Fps)↑
DPDETR [12]	90.10	-
DMM [56]	<u>87.97</u>	-
S <sup>2</sup> ANet [13]	142.80	-
TSFADet [50]	104.70	18.60
C <sup>2</sup> Former-S <sup>2</sup> ANet [49]	120.80	-
UA-CMDet [36]	234.00	9.12
MKD [18]	242.00	<u>42.30</u>
MGMF [41]	465.92	6.10
Ours	<b>17.07</b>	<b>43.10</b>

Table 3. Comparison of Frames Per Second (FPS) and parameter sizes of different methods on the DroneVehicle dataset. The methods involved correspond to Tab. 2.

sion images, particularly in challenging lighting conditions like low light or overexposure.

**Effect of ESTD module.** The ESTD module improves fine-grained detail capture through its specialized block, which adapts the Mamba architecture to optimize receptive fields for small target detection by strengthening local attention mechanisms. As shown in Fig. 10, incorporating the ESTD module into the baseline improves performance by +3.3%, demonstrating its effectiveness in enhancing small target detection accuracy.

**Effect of CARG module.** Our CARG module can better distinguish between complex backgrounds and targets. By assigning higher weights to key features of small targets and suppressing background channels, the CARG module boosts the model's anti-interference ability. As shown in Fig. 11, incorporating the CARG module into the base-

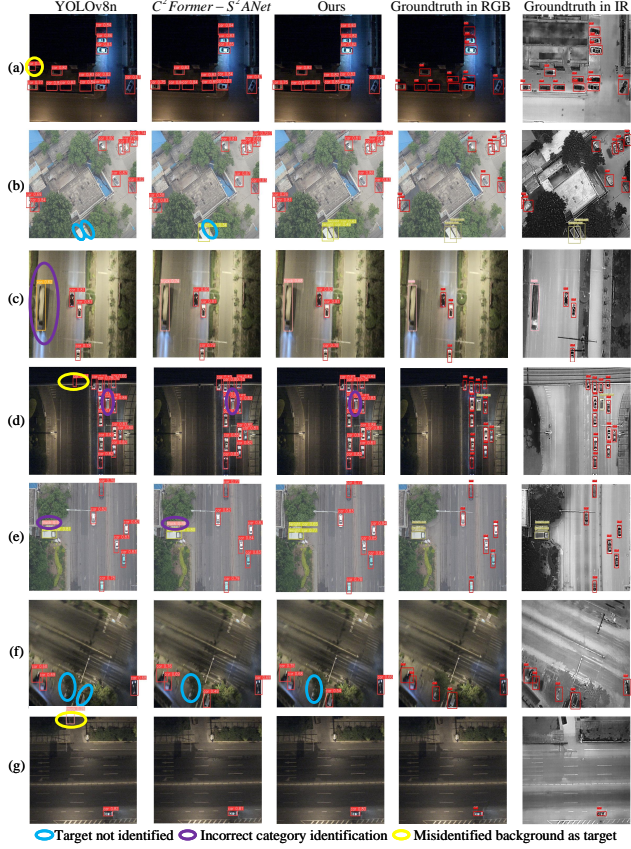


Figure 8. Visualization of experimental comparison plots and ground truth in infrared and visible modes in different scenarios. Specifically, we have selected five representative scenarios. (a): Night scenes with uneven light distribution (both overexposed and low light); (b) and (e): Daytime with plenty of light but complex backgrounds shaded by trees; (c): Night scenes with blurred targets due to high-speed acquisition and containing both large and small targets; (f): Multi-target and occluded night scenes; (g) and (d): Night scenes where the backgrounds also contain objects similar to the targets.

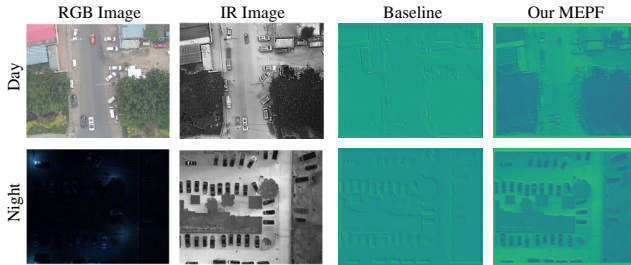


Figure 9. Comparison of feature map visualization between our MEPF module and the baseline pixel-level fusion method under different lighting conditions.

line improves performance by +3.4%.

As shown in Tab. 5, larger kernels have a slight superi-

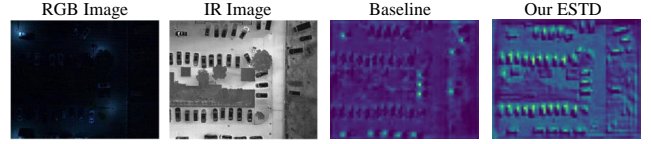


Figure 10. Comparison of feature map visualizations for our ESTD module and baseline approach.

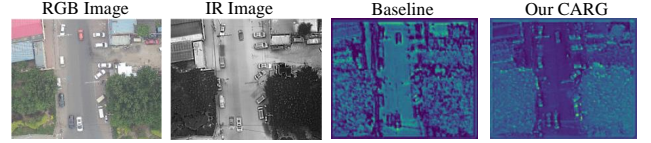


Figure 11. Comparison of feature map visualizations for our CARG module and the baseline approach.

Method	MEPF	ESTD	CARG	mAP <sub>50</sub> (%)↑	Parameter (MB) ↓
I				70.9	<b>11.49</b>
II	✓			73.8	11.50
III	✓	✓		74.2	16.61
IV	✓		✓	74.3	16.92
V	✓	✓	✓	<b>74.5</b>	17.07

Table 4. Ablation study on DroneVehicle. The best result is shown in **bold**. I: Baseline; II: Baseline+MEPF; III: Baseline+MEPF+ESTD; IV: Baseline+MEPF+CARG; V: Baseline+MEPF+ESTD+CARG.

Kernel size	Car	mAP <sub>50</sub> (%)↑	Parameter ↓
1 × 1	96.8	<b>74.5</b>	<b>4448887</b>
3 × 3	97.0	73.2	4449008
7 × 7	<b>97.4</b>	73.8	4449488

Table 5. Ablation on Spatial Attention Kernel Size.

ority in single vehicle recognition. However, considering overall accuracy and parameter size, the 1×1 kernel best balances performance and complexity. Thus we choose it.

## 5.6. Limitations

Our method, combining the MEPF and ESTVSS Block, achieves high small target detection accuracy with only 17.07MB parameters. However, it is less effective for larger targets, as shown in Tab. 2, where our overall accuracy on the DroneVehicle dataset lags behind DMM [56]. This is because DMM excels at detecting larger targets like Trucks and Vans, while our method is optimized for small targets like cars. On the VEDAI dataset, which has a smaller target size (as shown in Fig. 7), our method outperforms DMM. Future work will focus on designing a model capable of accurately detecting both large and small targets.

## 6. Conclusion

We propose the  $S_6^4$ -MSTD model, a novel selective structured state space model designed for multispectral-fused small target detection. Our approach introduces the MEPP module for efficient multispectral fusion, which achieves superior fusion quality with merely 1650 parameters. To further enhance the Mamba-based model's capability in small target detection, we introduce the ESTD and CARG modules, significantly improving the backbone's ability to capture subtle clues of small targets. Extensive experiments on the DroneVehicle and VEDAI datasets demonstrate the effectiveness of our method, which maintains an optimal balance between detection accuracy and suitability for lightweight deployment on edge devices.

## References

- [1] Yuhan Bai. Relu-function and derived function review. In *SHS Web of Conferences*, page 02006. EDP Sciences, 2022. 4
- [2] Pengguang Chen, Shu Liu, Hengshuang Zhao, and Jiaya Jia. Distilling knowledge via knowledge review. In *Proceedings of the IEEE/CVF conference on computer vision and pattern recognition*, pages 5008–5017, 2021. 7
- [3] Tianxiang Chen, Zhentao Tan, Tao Gong, Qi Chu, Yue Wu, Bin Liu, Jieping Ye, and Nenghai Yu. Mim-istd: Mamba-in-mamba for efficient infrared small target detection. *arXiv preprint arXiv:2403.02148*, 2024. 2
- [4] François Chollet. Xception: Deep learning with depthwise separable convolutions. In *Proceedings of the IEEE conference on computer vision and pattern recognition*, pages 1251–1258, 2017. 6
- [5] Tri Dao and Albert Gu. Transformers are ssms: Generalized models and efficient algorithms through structured state space duality. *arXiv:2405.21060*, 2024. 3
- [6] Alexey Dosovitskiy, Lucas Beyer, Alexander Kolesnikov, Dirk Weissenborn, Xiaohua Zhai, Thomas Unterthiner, Mostafa Dehghani, Matthias Minderer, Georg Heigold, Sylvain Gelly, Jakob Uszkoreit, and Neil Houlsby. An image is worth 16x16 words: Transformers for image recognition at scale. In *International Conference on Learning Representations*, 2021. 2
- [7] Stefan Elfving, Eiji Uchibe, and Kenji Doya. Sigmoid-weighted linear units for neural network function approximation in reinforcement learning. *Neural networks*, 107:3–11, 2018. 4, 5
- [8] Xinbo Gao, Mengjingcheng Mo, Haitao Wang, and Jiaxu Leng. Recent advances in small object detection. *Journal of Data Acquisition and Processing*, 36(3), 2021. 2, 6, 7
- [9] Mengyue Geng, Lin Zhu, Lizhi Wang, Wei Zhang, Ruiqin Xiong, and Yonghong Tian. Event-based visible and infrared fusion via multi-task collaboration. In *Proceedings of the IEEE/CVF Conference on Computer Vision and Pattern Recognition (CVPR)*, pages 26929–26939, 2024. 2
- [10] Albert Gu and Tri Dao. Mamba: Linear-time sequence modeling with selective state spaces. *arXiv preprint arXiv:2312.00752*, 2023. 3
- [11] Albert Gu, Karan Goel, and Christopher Ré. Efficiently modeling long sequences with structured state spaces. *arXiv preprint arXiv:2111.00396*, 2021. 3
- [12] Junjie Guo, Chenqiang Gao, Fangcen Liu, and Deyu Meng. Dpdetr: Decoupled position detection transformer for infrared-visible object detection. *arXiv preprint arXiv:2408.06123*, 2024. 7
- [13] Jiaming Han, Jian Ding, Jie Li, and Gui-Song Xia. Align deep features for oriented object detection. *IEEE transactions on geoscience and remote sensing*, 60:1–11, 2021. 7
- [14] Jiaming Han, Jian Ding, Nan Xue, and Gui-Song Xia. Redet: A rotation-equivariant detector for aerial object detection. In *Proceedings of the IEEE/CVF conference on computer vision and pattern recognition*, pages 2786–2795, 2021. 7
- [15] Kaiming He, Xiangyu Zhang, Shaoqing Ren, and Jian Sun. Deep residual learning for image recognition. In *2016 IEEE Conference on Computer Vision and Pattern Recognition (CVPR)*, pages 770–778, 2016. 2
- [16] Jie Hu, Li Shen, and Gang Sun. Squeeze-and-excitation networks. In *Proceedings of the IEEE conference on computer vision and pattern recognition*, pages 7132–7141, 2018. 5
- [17] Gao Huang, Zhuang Liu, Laurens Van Der Maaten, and Kilian Q. Weinberger. Densely connected convolutional networks. In *2017 IEEE Conference on Computer Vision and Pattern Recognition (CVPR)*, pages 2261–2269, 2017. 2
- [18] Zhanchao Huang, Wei Li, and Ran Tao. Multimodal knowledge distillation for arbitrary-oriented object detection in aerial images. In *ICASSP 2023-2023 IEEE International Conference on Acoustics, Speech and Signal Processing (ICASSP)*, pages 1–5. IEEE, 2023. 7
- [19] Touvron Hugo, Matthieu Cord, Douze Matthijs, Massa Francisco, Sablayrolles Alexandre, and Jegou Herve. Training data-efficient image transformers & distillation through attention. In *ICML*, 2021. 2
- [20] Sergey Ioffe and Christian Szegedy. Batch normalization: Accelerating deep network training by reducing internal covariate shift. In *International conference on machine learning*, pages 448–456. pmlr, 2015. 5
- [21] Mingi Ji, Byeongho Heo, and Sungrae Park. Show, attend and distill: Knowledge distillation via attention-based feature matching. In *Proceedings of the AAAI Conference on Artificial Intelligence*, pages 7945–7952, 2021. 7
- [22] Glenn Jocher, Ayush Chaurasia, and Jing Qiu. Ultralytics yolov8, 2023. 6, 7
- [23] Alex Krizhevsky, Ilya Sutskever, and Geoffrey E Hinton. Imagenet classification with deep convolutional neural networks. *Advances in neural information processing systems*, 25, 2012. 4
- [24] Minhyeok Lee. Gelu activation function in deep learning: a comprehensive mathematical analysis and performance. *arXiv preprint arXiv:2305.12073*, 2023. 5
- [25] Wentong Li, Yijie Chen, Kaixuan Hu, and Jianke Zhu. Oriented reppoints for aerial object detection. In *Proceedings of the IEEE/CVF conference on computer vision and pattern recognition*, pages 1829–1838, 2022. 7

- [26] Yuxuan Li, Qibin Hou, Zhaohui Zheng, Ming-Ming Cheng, Jian Yang, and Xiang Li. Large selective kernel network for remote sensing object detection. In *Proceedings of the IEEE/CVF International Conference on Computer Vision*, pages 16794–16805, 2023. 7
- [27] Min Lin, Qiang Chen, and Shuicheng Yan. Network in network. *arXiv preprint arXiv:1312.4400*, 2013. 4
- [28] Yuang Liu, Wei Zhang, and Jun Wang. Zero-shot adversarial quantization. In *2021 IEEE/CVF Conference on Computer Vision and Pattern Recognition (CVPR)*, pages 1512–1521, 2021. 7
- [29] Yue Liu, Yunjie Tian, Yuzhong Zhao, Hongtian Yu, Lingxi Xie, Yaowei Wang, Qixiang Ye, and Yunfan Liu. Vmamba: Visual state space model. *arXiv preprint arXiv:2401.10166*, 2024. 1, 2, 3, 7
- [30] Yu Oishi, Natsuki Yoshida, and Hiroyuki Oguma. Detecting moving wildlife using the time difference between two thermal airborne images. *Remote Sensing*, 16(8):1439, 2024. 1
- [31] Fang Qingyun and Wang Zhaokui. Cross-modality attentive feature fusion for object detection in multispectral remote sensing imagery. *Pattern Recognition*, 130:108786, 2022. 7
- [32] Sebastien Razakarivony and Frederic Jurie. Vehicle detection in aerial imagery: A small target detection benchmark. *Journal of Visual Communication and Image Representation*, 34:187–203, 2016. 6, 7
- [33] Kaijie Ren and Lei Zhang. Implicit discriminative knowledge learning for visible-infrared person re-identification. In *Proceedings of the IEEE/CVF Conference on Computer Vision and Pattern Recognition (CVPR)*, pages 393–402, 2024. 2
- [34] Jifeng Shen, Yifei Chen, Yue Liu, Xin Zuo, Heng Fan, and Wankou Yang. Icafusion: Iterative cross-attention guided feature fusion for multispectral object detection. *Pattern Recognition*, 145:109913, 2024. 7
- [35] Long Sun, Jiangxin Dong, Jinhui Tang, and Jinshan Pan. Spatially-adaptive feature modulation for efficient image super-resolution. In *Proceedings of the IEEE/CVF international conference on computer vision*, pages 13190–13199, 2023. 6
- [36] Yiming Sun, Bing Cao, Pengfei Zhu, and Qinghua Hu. Drone-based rgb-infrared cross-modality vehicle detection via uncertainty-aware learning. *IEEE Transactions on Circuits and Systems for Video Technology*, 32(10):6700–6713, 2022. 6, 7
- [37] Ilya Sutskever, James Martens, George Dahl, and Geoffrey Hinton. On the importance of initialization and momentum in deep learning. In *International conference on machine learning*, pages 1139–1147. PMLR, 2013. 6
- [38] Christian Szegedy, Wei Liu, Yangqing Jia, Pierre Sermanet, Scott Reed, Dragomir Anguelov, Dumitru Erhan, Vincent Vanhoucke, and Andrew Rabinovich. Going deeper with convolutions. In *2015 IEEE Conference on Computer Vision and Pattern Recognition (CVPR)*, pages 1–9, 2015. 2
- [39] Christian Szegedy, Wei Liu, Yangqing Jia, Pierre Sermanet, Scott Reed, Dragomir Anguelov, Dumitru Erhan, Vincent Vanhoucke, and Andrew Rabinovich. Going deeper with convolutions. In *Proceedings of the IEEE Conference on Computer Vision and Pattern Recognition (CVPR)*, 2015. 4, 5
- [40] Tushar Verma, Jyotsna Singh, Yash Bhartari, Rishi Jarwal, Suraj Singh, and Shubhkarmann Singh. Soar: Advancements in small body object detection for aerial imagery using state space models and programmable gradients. *arXiv preprint arXiv:2405.01699*, 2024. 2, 3
- [41] Simiao Wang, Chunpeng Wang, Chaoyi Shi, Yunan Liu, and Mingyu Lu. Mask-guided mamba fusion for drone-based visible-infrared vehicle detection. *IEEE Transactions on Geoscience and Remote Sensing*, 62:1–12, 2024. 1, 2, 3, 7
- [42] Xuewei Wang and Jun Liu. Vegetable disease detection using an improved yolov8 algorithm in the greenhouse plant environment. *Scientific Reports*, 14(1):4261, 2024. 1
- [43] Zeyu Wang, Chen Li, Huiying Xu, and Xinzhong Zhu. Mamba yolo: Ssms-based yolo for object detection. *arXiv preprint arXiv:2406.05835*, 2024. 1
- [44] Shufang Xu, Xu Chen, Haiwei Li, Tianci Liu, Zhonghao Chen, Hongmin Gao, and Yiyan Zhang. Airborne small target detection method based on multimodal and adaptive feature fusion. *IEEE Transactions on Geoscience and Remote Sensing*, 62:1–15, 2024. 3
- [45] Bin Yang, Jun Chen, and Mang Ye. Shallow-deep collaborative learning for unsupervised visible-infrared person re-identification. In *Proceedings of the IEEE/CVF Conference on Computer Vision and Pattern Recognition (CVPR)*, pages 16870–16879, 2024. 2
- [46] Linli Yao, Lei Li, Shuhuai Ren, Lean Wang, Yuanxin Liu, Xu Sun, and Lu Hou. Deco: Decoupling token compression from semantic abstraction in multimodal large language models. *arXiv preprint arXiv:2405.20985*, 2024. 6
- [47] Hao Yi, Bo Liu, Bin Zhao, and Enhai Liu. Small object detection algorithm based on improved yolov8 for remote sensing. *IEEE Journal of Selected Topics in Applied Earth Observations and Remote Sensing*, 17:1734–1747, 2024. 3
- [48] Weihao Yu and Xinchao Wang. Mambaout: Do we really need mamba for vision? *arXiv preprint arXiv:2405.07992*, 2024. 2
- [49] Maoxun Yuan and Xingxing Wei. C 2 former: Calibrated and complementary transformer for rgb-infrared object detection. *IEEE Transactions on Geoscience and Remote Sensing*, 2024. 2, 7
- [50] Maoxun Yuan, Yinyan Wang, and Xingxing Wei. Translation, scale and rotation: cross-modal alignment meets rgb-infrared vehicle detection. In *European Conference on Computer Vision*, pages 509–525. Springer, 2022. 7
- [51] Jiaqing Zhang, Jie Lei, Weiying Xie, Zhenman Fang, Yunsong Li, and Qian Du. Superyolo: Super resolution assisted object detection in multimodal remote sensing imagery. *IEEE Transactions on Geoscience and Remote Sensing*, 61:1–15, 2023. 2, 3, 4, 7
- [52] Jiaqing Zhang, Jie Lei, Weiying Xie, Yunsong Li, Geng Yang, and Xiuping Jia. Guided hybrid quantization for object detection in remote sensing imagery via one-to-one self-teaching. *IEEE Transactions on Geoscience and Remote Sensing*, 2023. 7

- [53] Yin Zhang, Mu Ye, Guiyi Zhu, Yong Liu, Pengyu Guo, and Junhua Yan. Ffca-yolo for small object detection in remote sensing images. *IEEE Transactions on Geoscience and Remote Sensing*, 62:1–15, 2024. [3](#)
- [54] Sijie Zhao, Hao Chen, Xueliang Zhang, Pengfeng Xiao, Lei Bai, and Wanli Ouyang. Rs-mamba for large remote sensing image dense prediction. *IEEE Transactions on Geoscience and Remote Sensing*, 62:1–14, 2024. [2](#)
- [55] Naishan Zheng, Man Zhou, Jie Huang, Junming Hou, Haoying Li, Yuan Xu, and Feng Zhao. Probing synergistic high-order interaction in infrared and visible image fusion. In *Proceedings of the IEEE/CVF Conference on Computer Vision and Pattern Recognition (CVPR)*, pages 26384–26395, 2024. [2](#)
- [56] Minghang Zhou, Tianyu Li, Chaofan Qiao, Dongyu Xie, Guoqing Wang, Ningjuan Ruan, Lin Mei, and Yang Yang. Dmm: Disparity-guided multispectral mamba for oriented object detection in remote sensing. *arXiv preprint arXiv:2407.08132*, 2024. [2](#), [7](#), [8](#)
- [57] Lianghui Zhu, Bencheng Liao, Qian Zhang, Xinlong Wang, Wenyu Liu, and Xinggang Wang. Vision mamba: Efficient visual representation learning with bidirectional state space model. In *ICML*, 2024. [2](#)